Ab Initio Molecular Dynamics Simulation of the Energy-Relaxation Process of the Protonated Water Dimer

Yusuke Yamauchi, Shiho Ozawa, and Hiromi Nakai*

Department of Chemistry, School of Science and Engineering, Waseda University, Tokyo 169-8555, Japan

Received: October 6, 2006; In Final Form: January 22, 2007

Relaxation processes of the energy-rich protonated water dimer $H^+(H_2O)_2$ were investigated by the ab initio molecular dynamics (AIMD) method. At first, the energy-rich $H^+(H_2O)_2$ was reproduced by simulating a collision reaction between the protonated water monomer H_3O^+ and H_2O. Next it was collided with N_2 in order to observe the effects of intramolecular vibration redistribution and intermolecular energy transfer. Forty-eight AIMD simulations of the collision of $H^+(H_2O)_2$ with N_2 were performed by changing the initial orientation and the time interval between two collisions. It was revealed that the amount of energy transferred from $H^+(H_2O)_2$ to N_2 decreased the longer the time interval. The relationship between the intermolecular energy transfer and the vibrational states was examined with the use of an energy-transfer spectrogram (ETS), which is an analysis technique combining energy density analysis and short-time Fourier transform. The ETS demonstrates a characteristic vibrational mode for the energy transfer, which corresponds to the stretching of the hydrogen bond between $H^+(H_2O)_2$ and N_2 in an active complex.

Introduction

For the theoretical investigation of various environmental phenomena, for example, chemistry in the atmosphere, combustion, and aerial pollution, numerous elementary reaction steps have to be taken into consideration.[1−3] Reaction products of the elementary steps have excess energy, and lopsided distributions of energy frequently occur. The fact that these steps proceed in the nonequilibrium state complicates our understanding of the reaction dynamics. Ab initio molecular dynamics (AIMD) simulation is one of the most powerful tools for computational reproduction of the nonequilibrium state.[4−7] It is equivalent to following the motion of nuclei on the potential hypersurface obtained by electronic structure calculation. The electronic structure calculation is practically performed "on the fly" in the AIMD method.

Recently, we proposed an analysis technique for the AIMD simulation, which is termed an energy-transfer spectrogram (ETS)[8] and was developed in order to display the vibrational modes through which energy is transferred during a reaction step. This technique consists of two methods (i.e., the energy-partitioning method and time-frequency analysis). The former is necessary to examine directly how local energy is transferred. Localizing the electronic energy is generally known as a complicated operation because the energy is a unique property of a system. We selected the energy density analysis (EDA) method developed by Nakai[9] as an energy-partitioning method. The latter displays the relationship between energy transfer and molecular vibration visibly on the time-frequency map. It has been used in some studies to analyze molecular dynamics.[10−12] Short-time Fourier transform (ST-FT) was applied for this purpose.

In this study, the relaxation processes of the $H^+(H_2O)_2$ energy-rich protonated water dimer were studied by AIMD and ETS. The $H^+(H_2O)_n$ protonated water cluster is a typical hydrogen-bonded cluster in the atmosphere,[13] where n indicates the size of the cluster ion. The crystal growth of $H^+(H_2O)_n$ is related to various phenomena (e.g., the aerial pollution mechanism and the efficiency of semiconductor manufacturing), which have been studied by many researchers.[14−16] Okada and co-workers[17,18] studied the size-increasing mechanism between $H^+(H_2O)_n$ ($n = 1-10$) and H_2O by using guided ion beam tandem mass spectrometry. The process, in which the n-mer ion becomes an $(n+1)$-mer ion, is classified into three steps: collision, chemical adsorption, and relaxation.

The objective of the present study is to elucidate the mechanism of the energy-relaxation process in an energy-rich protonated water cluster using the ETS. This article consists of four sections. Section 2 mentions the computational methods of the present investigation for the collision between hot $H^+(H_2O)_2$ and N_2. The results of the AIMD simulation and its analysis by the ETS are shown in section 3. The peaks appearing in the ETS are discussed as compared to the frequencies of normal vibrational modes. Finally, we summarize the present study in section 4.

Computational Details

The present study investigated the relaxation process of the excess energy in the crystal growth of $H^+(H_2O)_n$ ($n = 1 \rightarrow 2$). To deal with the intramolecular and intermolecular energy-transfer phenomenon, the three-body reaction of H_3O^+, H_2O, and N_2 was considered. The procedure follows the two-step Lindemann mechanism, which is often used in molecular dynamics.[19] The first step is the formation of $H^+(H_2O)_2$* by combining H_3O^+ and H_2O:

$$H_3O^+ + H_2O \rightarrow H^+(H_2O)_2^* \qquad (1)$$

Here, the asterisk (*) means that the $H^+(H_2O)_2$ product is vibrationally excited as a result of the binding energy between H_3O^+ and H_2O. The second step is a relaxation of the excess

* To whom correspondence should be addressed. E-mail: nakai@waseda.jp.

10.1021/jp066570o CCC: $37.00
Published on Web 02/28/2007

energy of $H^+(H_2O)_2$ by colliding with N_2:

$$H^+(H_2O)_2^* + N_2 \rightarrow H^+(H_2O)_2 + N_2^* \quad (2)$$

To simulate these processes, we performed the following AIMD simulations:

Step (i): Adjusting the internal energies to 300 K, which corresponds to 1.1 times the zero-point energies (ZPEs) to H_3O^+ and H_2O, we performed 2.0 ps simulations for equilibration. Similarly, simulation for equilibration was performed for N_2.

Step (ii): Equilibrated H_3O^+ approached equilibrated H_2O with a collision energy of 0.5 eV from a distance of 15 Å. The bond energy between H_3O^+ and H_2O in $H^+(H_2O)_2$ is 2.77 eV. Several trajectories were examined by changing the initial orientations of these two molecules. We selected one trajectory in which $H^+(H_2O)_2$ is generated and its lifetime is long enough to use the simulation for N_2 collision.

Step (iii): Equilibrated N_2 approached $H^+(H_2O)_2$ generated in step (ii) with a collision energy of 0.1 eV from a distance of 10 Å. The bond energy between $H^+(H_2O)_2$ and N_2 in their complex is 0.44 eV. Forty-eight simulations were performed with different initial orientations of $H^+(H_2O)_2$ and N_2 and at different simulation times (ii).

All of the AIMD simulations were carried out under the microcanonical ensemble. The velocity Verlet method with a time step of 0.25 fs was adopted as the numerical integration algorithm for the equation of motion (EOM).

The potential energy and atomic force were estimated by the DFT calculation with the B3LYP functional,[20] which consists of the HF or exact exchange, the Slater exchange,[21] the Becke (B88) exchange,[22] the Vosko−Wilk−Nusair (VWN5) correlation,[23] and the Lee−Yang−Parr (LYP) correlation[24] functionals. Duning's valence double-ζ (D95V)[25] basis sets were used for the DFT calculation. The DFT calculation was performed with the GAMESS program package.[26] The computational level was selected for practical reasons. To check the accuracy of the computational level, we calculated the bond energies of $H^+(H_2O)_2$ obtained by various methods. The energies using B3LYP/D95V and the second-order Møller-Plesset perturbation theory (MP2) with aug-cc-pVTZ[27,28] are 2.79 (2.73) and 2.30 (2.29) eV, respectively, where values in parentheses contain the basis set superposition error (BSSE) correction. However, the CPU times of the MP2/aug-cc-pVTZ calculations are about 140 times as long as those of the B3LYP/D95V ones. For more details, see the Appendix.

Nuclear kinetic energy T_i was calculated using nuclear mass and the velocity obtained by the AIMD simulation, whereas atomic potential energy V_i was estimated by the EDA method. Namely, the kinetic energy density is evaluated as follows

$$\mathcal{T}_i^S = \sum_{\mu\in i}\sum_{\nu} P_{\mu\nu}\left\langle \chi_\nu \middle| -\frac{1}{2}\nabla^2 \middle| \chi_\mu \right\rangle \equiv \sum_{\mu\in i}\sum_{\nu} P_{\mu\nu}T_{\nu\mu} = \sum_{\mu\in i}(\mathbf{PT})_{\mu\mu} \quad (3)$$

where **P** is the density matrix with an atomic orbital (AO) basis. Nuclear attraction and Coulomb and exact exchange-energy densities are divided in a similar way. The exchange-correlation energy density is estimated by using the grid technique. The nuclear repulsion energy density is shared half-and-half by the two atoms. One can find more detailed information in ref 9. The EDA calculation was performed by linking our original code with the GAMESS package.

Because the present study investigated the energy transfer between $H^+(H_2O)_2$ and N_2, the partial sum of the atomic energy E_i was obtained for $H^+(H_2O)_2$ and N_2, respectively:

$$E_{H^+(H_2O)_2} = \sum_{i\in H^+(H_2O)_2} E_i \quad (4)$$

$$E_{N_2} = \sum_{i\in N_2} E_i \quad (5)$$

To obtain ETS, we evaluated the time-correlation functions of the total energy variations for $H^+(H_2O)_2$ and N_2: $\langle \dot{E}_{H^+(H_2O)_2}(t)\cdot \dot{E}_{H^+(H_2O)_2}(t+\tau)\rangle$ and $\langle \dot{E}_{N_2}(t)\cdot \dot{E}_{N_2}(t+\tau)\rangle$. Because the sum of $E_{H^+(H_2O)_2}$ and E_{N_2} is constant, we can write

$$\dot{E}_{H^+(H_2O)_2} = -\dot{E}_{N_2} \quad (6)$$

Therefore, these time-correlation functions are equivalent to each other.

$$\langle \dot{E}_{H^+(H_2O)_2}(t)\cdot \dot{E}_{H^+(H_2O)_2}(t+\tau)\rangle = \langle \dot{E}_{N_2}(t)\cdot \dot{E}_{N_2}(t+\tau)\rangle \quad (7)$$

The present study uses a Hanning window[29] with $\tau = 0.5$ ps expressed as

$$h(t'-t) = \begin{cases} \frac{1}{2} - \frac{1}{2}\cos\left\{\frac{\pi(t'-t+\tau)}{\tau}\right\} & \text{for } -\tau \le t'-t \le \tau \\ 0 & \text{otherwise} \end{cases} \quad (8)$$

The window length τ is related to the resolution of frequency ω in the ST-FT given by

$$S(t,\omega) = \frac{1}{2\pi}\int_{-\infty}^{\infty} f(t,t')\, h(t'-t)\exp(-i\omega t')\, dt' \quad (9)$$

because of the uncertainty in the time-frequency analysis. The resolution of $S(t, \omega)$ using the time-correlation function $\langle \dot{E}_{N_2}(t)\cdot \dot{E}_{N_2}(t+\tau)\rangle$, that is, ETS, was obtained by the original code.

Results and Discussion

At first, we show the time evolution of the molecular geometry in the AIMD simulation. Figure 1 a,b shows two trajectories of the simulations in step (iii), which are explained in section 3. The solid line indicates the distance between H_3O^+ and H_2O in $H^+(H_2O)_2$. The dashed line is the distance between $H^+(H_2O)_2$ and N_2. t^{int} means the time interval between two collisions, that is, the collision of H_3O^+ with H_2O and the collision of $H^+(H_2O)_2$ with N_2. The time interval is 0.14 ps in Figure 1a. This means that the collision between $H^+(H_2O)_2$ and N_2 occurred immediately after the protonated water dimer was generated. Therefore, when N_2 collided with $H^+(H_2O)_2$, the intramolecular vibration in the dimer ion could not yet be sufficiently redistributed. However, the time interval in Figure 1b is 3.27 ps, and thus the vibrational energy in $H^+(H_2O)_2$ could spread more extensively than in the former case. Actually, the difference in the time interval affects the behavior of the solid line after the collision in Figure 1. In Figure 1a, the maximum distance between H_3O^+ and H_2O after the collision is 5.4 Å at 3.5 ps. However, the maximum value in Figure 1b is 3.5 Å at 1.4 ps.

Figure 2 shows the dependency on the time interval of the energy transferred from N_2 to $H^+(H_2O)_2$ by the collision. The minus sign accompanying the energy term means that the energy moves from $H^+(H_2O)_2$ to N_2. The rectangular plots correspond

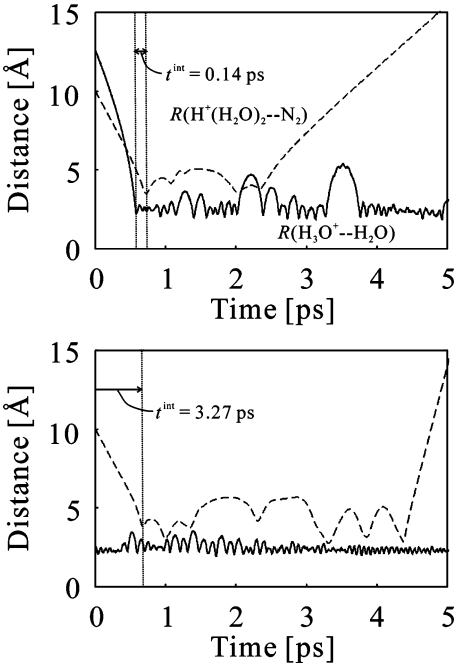

Figure 1. Time change of the distances between the ion and molecule in two trajectories of the AIMD simulation. The solid line and the broken line indicate the distances $R(H_3O^+-H_2O)$ and $R(H^+(H_2O)_2-N_2)$, respectively.

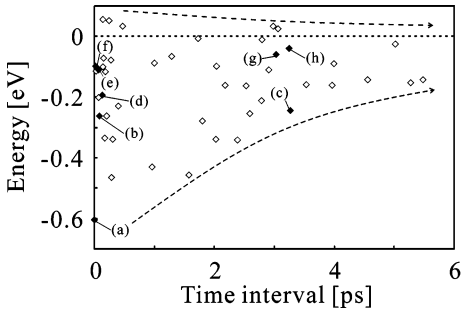

Figure 2. Energy differences in $H^+(H_2O)_2$ before and after the collision with N_2 for the 48 simulation trajectories. The time interval is the length from the collision between H_3O^+ and H_2O to the collision between $H^+(H_2O)_2$ and N_2. The black dots in a−h are trajectories corresponding to those in Figure 3a−h.

to the results of the 48 simulations in step (iii) of the previous section. The transferred energy does not include the translational energy. The average value of the 48 energies is −0.17 eV. Thus, N_2 took the excess vibrational energy out of the dimer ion. Just after the incorporation of H_2O into H_3O^+, when the time interval is short, the transferred energy is widely spread from −0.60 to 0.05 eV. The longer the time interval, the smaller the spread of the transferred energy. The average values of the energies of $(0 < t^{int} \leq 2)$, $(2 < t^{int} \leq 4)$, and $(4 < t^{int} \leq 6)$ ps are −0.19, −0.14, and −0.12 eV, respectively. It is clear that the effect of intermolecular energy transfer on energy relaxation decreases because of an increasing intramolecular vibrational relaxation effect. Of course, this remark is not universal; for example, it is not applicable to a case in which dissociation occurs because of high collision energy.

The relation of vibrational states to the energy transfer was investigated by the ETS technique. Eight trajectories were chosen from the 48 trajectories as samples, which are marked in Figure 2. The transferred energies of these sample trajectories are (a) −0.60, (b) −0.26, (c) −0.24, (d) −0.19, (e) −0.11, (f) −0.10, (g) −0.06, and (h) −0.04 eV. We show three kinds of information in Figure 3. First, the time development of the

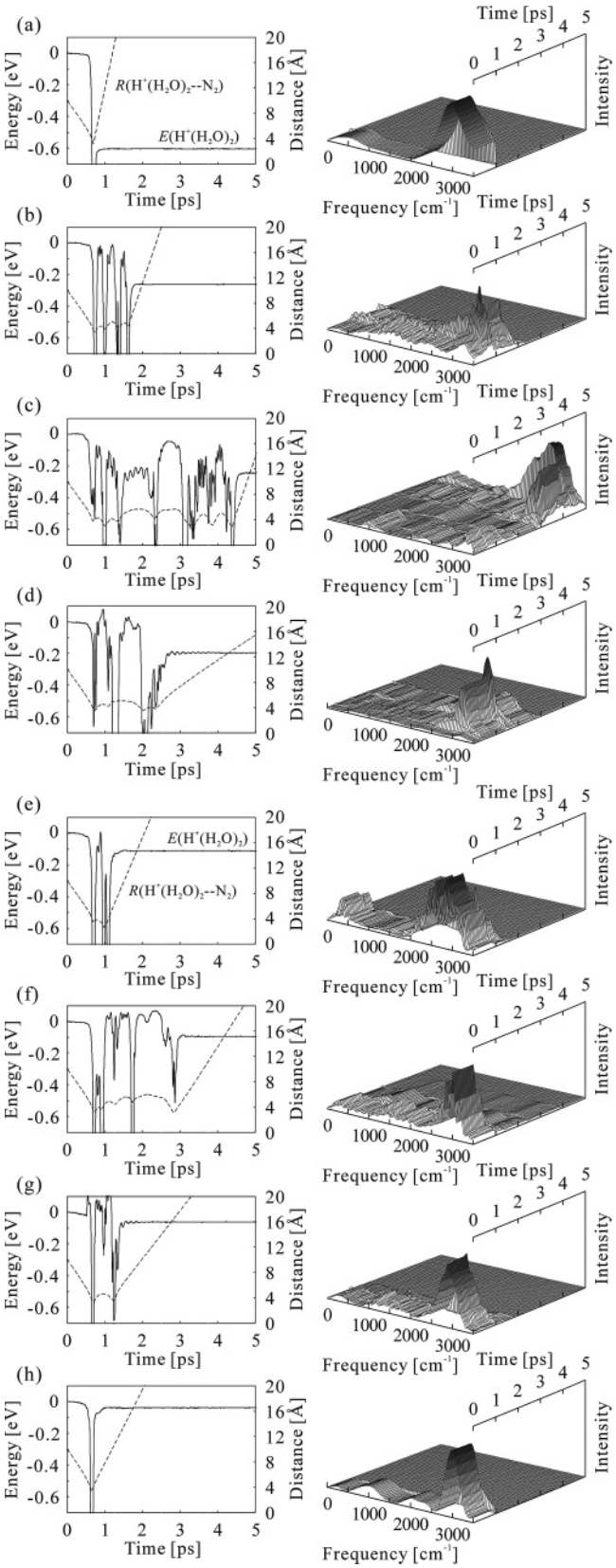

Figure 3. Analysis results of eight trajectories of the AIMD simulation. The left-hand side shows the time changes of the distance between $H^+(H_2O)_2$ and N_2 (broken line) and the energy in $H^+(H_2O)_2$ (solid line). The right-hand side shows the ETS.

distance between $H^+(H_2O)_2$ and N_2 is shown on the left-hand side as the broken line. Second, the time development of the energy of $H^+(H_2O)_2$ is also shown on the left-hand side as the solid line. This change in energy corresponds to the value of

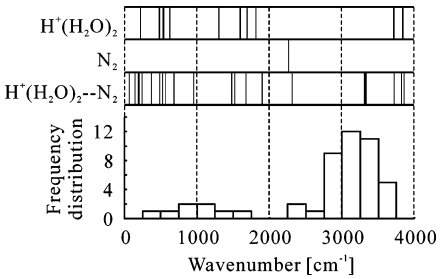

Figure 4. Harmonic frequencies of $H^+(H_2O)_2$, N_2, and active complex $H^+(H_2O)_2-N_2$ calculated at the same computational level as used in the AIMD simulation. The frequency of 3328 cm^{-1}, which is a stretching vibration of the hydrogen bond between $H^+(H_2O)_2$ and N_2, is accented by the heavy line. The frequency distribution graph of maximum peaks in the 48 spectrograms is given below.

the energy in Figure 2. For example, the energy went from 0 to −0.60 eV in Figure 3a. Third, the ETS is shown on the right-hand side as a 3D map.

Let us discuss the left-hand side of Figure 3. When the distance is long, the time change of the energy is flat. This indicates that energy transfer between $H^+(H_2O)_2$ and N_2 does not occur at a long separation because of a weak interaction. However, the energy curve oscillates significantly in the interacting region. In this region, it seems that there is no decided tendency in the manner of oscillation, so the ETS was used to examine the energy-transfer dynamics from the time−frequency point of view. The ETS has three axes consisting of frequency, time, and intensity. The ETS surface is flat outside the field of the strong-interaction region. Remarkable peaks appear upon collision. It is interesting that the wavenumbers of the strong vibration in a−h, namely, 3001, 3210, 2918, 3043, 2834, 3085, 2959, and 3043 cm^{-1}, are quite similar in spite of the diversity of energy behavior. This suggests that one or more particular molecular vibrations relate to the energy-relaxation mechanism.

Normal-mode analysis was performed to assign the characteristic vibration. Figure 4 shows the harmonic molecular vibrations of $H^+(H_2O)_2$, N_2, and $H^+(H_2O)_2-N_2$ calculated at the same computational level as used in the AIMD simulation. The remarkable peaks in the eight ETSs are located in the frequency region from 2500 to 3500 cm^{-1}. There is no vibrational mode in this region of $H^+(H_2O)_2$ and N_2. However, there is a mode at 3328 cm^{-1} for the active complex of $H^+(H_2O)_2-N_2$. It is a stretching vibration of the hydrogen bond between $H^+(H_2O)_2$ and N_2. The frequency distribution of the maximum peaks in 48 trajectories is shown at the bottom of Figure 4. This Figure indicates that 33 trajectories (∼70%) have peaks in the range of 2500−3500 cm^{-1}. Therefore, we conclude that the energy transfer from one molecule to another is clearly concerned with the generated vibration of an active complex.

Concluding Remarks

As a model study of the crystal growth of a cluster, AIMD simulations of the vibration relaxation process of $H^+(H_2O)_2$ were performed. At first, the vibrationally excited $H^+(H_2O)_2$ was yielded by a simulation of the collision reaction between H_3O^+ and H_2O. To complete the growth step, the cluster ion needs to relax for energy stabilization by IVR and/or intermolecular energy transfer. N_2 was used as a partner molecule for energy transfer. Thus, energy-rich $H^+(H_2O)_2$ was collided with N_2 in the second simulation. Many simulations were performed with different initial orientations and different time intervals between two collisions. It was found that a long time interval leads to small transferred energy from $H^+(H_2O)_2$ to N_2. Namely, the IVR progression reduces the effect of intermolecular energy transfer to energy relaxation. Next, we applied our analysis technique, termed ETS, to the relaxation mechanism. ETS clarified a characteristic vibration in the energy-transfer dynamics. When we compared the vibration with harmonic vibrational modes, it was clear that the important mode was the stretching of the hydrogen bond between $H^+(H_2O)_2$ and N_2 in an active complex. ETS revealed the relation of molecular vibration to energy relaxation in the present study. Other applications of ETS will be reported elsewhere.

Acknowledgment. We are grateful to Professor Yoshiki Okada for invaluable discussions. This study was supported in part by the 21st century Center Of Excellence (21COE) (Practical Nano-Chemistry) from the Japanese Ministry of Education, Culture, Sports, Science, and Technology (MEXT), the Next Generation Super Computing Project, Nanoscience Program, of MEXT, a Grant-in-Aid for Scientific Research on Priority Areas (Molecular Theory for Real Systems) (KAKENHI 18066016) from MEXT, and a project research grant (Development of a High-Performance Computational Environment for Quantum Chemical Calculation and its Assessment) from the Advanced Research Institute for Science and Engineering (RISE) of Waseda University.

Appendix

Electronic structure calculations at the B3LYP/D95V level were used in the present molecular dynamics simulations. This Appendix assesses the accuracy of the adopted computational method. Table 1 shows the energetics calculated with several methods, namely, DFT calculations using the B3LYP functional with STO-6G,[30] D95V,[25] and aug-cc-pVTZ[27,28] basis sets and the MP2 calculations with the aug-cc-pVTZ basis sets as well as their CPU times. Bond energies of $H_2O-H_3O^+$ and $H^+(H_2O)_2-N_2$ were calculated. All molecular geometries are optimized once at the B3LYP/6-311+G(2df, pd)[31,32] level. BSSE correction is performed by the counterpoise method.[33]

Using a sufficiently large basis function (e.g., aug-cc-pVTZ), we find that the deviations of the B3LYP results with respect to the MP2 ones become very small: 0.03 and −0.01 kcal/mol for the bond energies of $H_3O^+-H_2O$ and $H^+(H_2O)_2-N_2$, respectively. Although the computational costs of the B3LYP/aug-cc-pVTZ calculations are about one-third of the MP2/aug-cc-pVTZ ones, about 6 months is needed to carry out the 10 000 steps in the AIMD simulation. However, the CPU times of STO-6G and D95V are comparable and very reasonable. The energetics using D95V are somewhat better than those using STO-6G. The errors in the bond energies of $H_3O^+-H_2O$ and $H^+(H_2O)_2-N_2$ using D95V are 0.44 and 0.14 eV, respectively.

TABLE 1: Bond Energies between H_3O^+ and H_2O and between $H^+(H_2O)_2$ and N_2[a]

	$E^{bond}(H_3O^+-H_2O)$ (eV)	$E^{bond}(H^+(H_2O)_2-N_2)$ (eV)	CPU time s/step	CPU time day/10 000 steps
B3LYP/STO-6G	3.47 (1.18)	0.46 (0.15)	27.6	3.2
B3LYP/D95V	2.73 (0.44)	0.44 (0.14)	30.3	3.5
B3LYP/aug-cc-pVTZ	2.32 (0.03)	0.29 (−0.01)	1438.9	166.5
MP2/aug-cc-pVTZ	2.29 (---)	0.30 (---)	4232.8	489.9

[a] These values were obtained using DFT with the B3LYP functional and basis set super error correction method. Costs for the force calculation were estimated on a Pentium 4/3.0GHz central processing unit.

TABLE 2: Comparison of Normal-Mode Frequencies of the $H^+(H_2O)_2-N_2$ Complex Obtained by MP2/aug-cc-pVTZ, B3LYP/D95V, and B3LYP/aug-cc-pVTZ[a]

	B3LYP		MP2
	D95V (cm^{-1})	aug-cc-pVTZ (cm^{-1})	aug-cc-pVTZ (cm^{-1})
1	67.7 (19.4)	50.3 (2.0)	48.2
2	140.8 (30.1)	112.9 (2.2)	110.8
3	179.4 (44.9)	138.5 (4.1)	134.5
4	192.1 (48.4)	145.4 (1.7)	143.7
5	236.7 (44.7)	186.2 (5.7)	192.0
6	380.6 (51.3)	304.7 (24.6)	329.3
7	480.8 (134.2)	327.4 (19.2)	346.6
8	519.3 (65.7)	453.8 (0.2)	453.6
9	568.0 (93.0)	472.8 (2.3)	475.1
10	687.9 (103.0)	570.6 (14.4)	584.9
11	962.8 (219.7)	708.8 (34.3)	743.1
12	1481.1 (139.5)	1321.8 (19.8)	1341.5
13	1520.8 (17.4)	1452.2 (51.1)	1503.3
14	1674.9 (27.5)	1612.9 (34.5)	1647.4
15	1714.5 (5.6)	1682.7 (26.2)	1708.9
16	1905.0 (18.4)	1864.8 (58.7)	1923.4
17	2318.4 (121.3)	2463.1 (266.0)	2197.0
18	3328.2 (111.0)	3392.0 (47.3)	3439.3
19	3731.2 (36.2)	3750.4 (17.0)	3767.4
20	3822.1 (33.0)	3765.6 (23.5)	3789.1
21	3863.7 (8.1)	3837.9 (34.0)	3871.9
MAD	(65.4)	(32.8)	

[a] Absolute deviations between MP2 and B3LYP are shown in parentheses.

Next, we examine the vibrational frequencies of $H^+(H_2O)_2-N_2$ calculated at the B3LYP/D95V, B3LYP/aug-cc-pVTZ, and MP2/aug-cc-pVTZ levels. Differences between the B3LYP and the MP2 results are shown in parentheses. Mean absolute deviations of B3LYP/D95V and aug-cc-pVTZ are 65.4 and 32.8 cm^{-1}, respectively. The frequency resolution of the ETS using a 0.5 ps window length is 66.7 cm^{-1}. Therefore, we think that the accuracy at the B3LYP/D95V level is acceptable for the present subject. In particular, the vibrational mode related to the energy transfer, which is in the range of 2500−3500 cm^{-1} as discussed in the text, is commonly assigned to the 18th mode by these methods.

References and Notes

(1) May, V.; Kuhn, O. *Charge and Energy Transfer Dynamics in Molecular Systems*; Wiley-VCH: Weinheim, Germany, 2004.

(2) Uzer, T.; Miller, W. H. *Phys. Lett.* **1991**, *199*, 73.

(3) Owrutsky, J. C.; Raftery, D.; Hochstrasser, R. M. *Annu. Rev. Phys. Chem.* **1994**, *45*, 519.

(4) Marx, D.; Hutter J. Ab-initio Molecular Dynamics: Theory and Implementation. In *Modern Methods and Algorithms in Quantum Chemistry*; NIC Series; Forschungzentrum: Juelich, 2000; Vol. 1.

(5) Tuckerman, M. E. *J. Phys.: Condens. Matter* **2002**, *14*, 1297.

(6) Nakai, H.; Yamauchi, Y.; Matsuda, A.; Okada, Y.; Takeuchi, K. *J. Mol. Struct.: THEOCHEM* **2002**, *592*, 61.

(7) Nakai, H.; Yamauchi, Y.; Nakata, A.; Baba, T.; Takahashi, H. *J. Chem. Phys.* **2003**, *119*, 4223.

(8) Yamauchi, Y.; Nakai, H. *J. Chem. Phys.* **2005**, *123*, 034101.

(9) Nakai, H. *Chem. Phys. Lett.* **2002**, *363*, 73.

(10) Askar, A.; Cetin, A. E.; Rabitz, H. *J. Phys. Chem.* **1996**, *100*, 19165.

(11) Yamauchi, Y.; Nakai, H.; Okada, Y. *J. Chem. Phys.* **2004**, *121*, 11098.

(12) Bach, A.; Hostettler, J. M.; Chen, P. *J. Chem. Phys.* **2005**, *123*, 021101.

(13) Harrison, R. G.; Carslaw, K. S. *Rev. Geophys.* **2003**, *41*, 1.

(14) Niedner-Schatteburg, G.; Bondybey, V. E. *Chem. Rev.* **2000**, *100*, 4059.

(15) Jiang, J. C.; Wang, Y. S.; Chang, H. C.; Lin, S. H.; Lee, Y. T.; Niedner-Schatteburg, G.; Chang, H. C. *J. Am. Chem. Soc.* **2000**, *122*, 1398.

(16) Honma, K.; Sunderlin, L. S.; Armentrout, P. B. *Int. J. Mass Spectrom. Ion Processes* **1992**, *117*, 237.

(17) Yamaguchi, S.; Kudoh, S.; Okada, Y.; Orii, T.; Takeuchi, K. *Chem. Phys. Lett.* **2002**, *359*, 480.

(18) Yamaguchi, S.; Kudoh, S.; Okada, Y.; Orii, T.; Takeuchi, K.; Ichikawa, T.; Nakai, H. *J. Phys. Chem. A* **2003**, *107*, 10904.

(19) Martin, D. L.; Thompson, D. L.; Raff, L. M. *J. Chem. Phys.* **1986**, *84*, 4426.

(20) Becke, A. D. *J. Chem. Phys.* **1993**, *98*, 5648.

(21) Slater, J. C. *Phys. Rev.* **1951**, *81*, 385.

(22) Becke, A. D. *Phys. Rev. A* **1988**, *38*, 3098.

(23) Vosko, S. H.; Wilk, L.; Nusair, M. *Can. J. Phys.* **1980**, *58*, 1200.

(24) Lee, C.; Yang. W.; Parr, R. G. *Phys. Rev. B* **1988**, *37*, 785.

(25) Dunning Jr., T. H.; Hay, P. J. *Modern Theoretical Chemistry*; Plenum: New York, 1976.

(26) Schmidt, M. W.; Baldrige, K. K.; Boatz, J. A.; Elbert, S. T.; Gordon, M. S.; Jensen, J. H.; Koseki, S.; Matsunaga, N.; Nguyen, K. A.; Su, S. J.; Windus, T. L.; Depois, M.; Montgomery, J. A. *J. Comput. Chem.* **1993**, *14*, 1347.

(27) Dunning, T. H., Jr. *J. Chem. Phys.* **1989**, *90*, 1007.

(28) Woon, D. E.; Dunning, T. H., Jr. *J. Chem. Phys.* **1993**, *98*, 1358.

(29) Percival, D. B.; Walden, A. T. *Spectral Analysis for Physical Applications: Multitaper and Conventional Univariate Techniques*; Cambridge University Press: Cambridge, U.K., 1993.

(30) Hehre, W. J.; Stewart, R. F.; Pople, J. A. *J. Chem. Phys.* **1969**, *51*, 2657.

(31) Krishnan, R.; Binkley, J. S.; Seeger, R.; Pople, J. A. *J. Chem. Phys.* **1980**, *72*, 650.

(32) Clark, T.; Chandrasekhar, J.; Schleyer, P. V. R. *J. Comput. Chem.* **1983**, *4*, 294.

(33) Simon, S.; Duran, M.; Dannenberg, J. J. *J. Chem. Phys.* **1996**, *105*, 11024.